GAN-Based Generation of Pre-Disaster SAR for Earthquake Interferometry

Kohei Arai, Kengo Ohiwane, Hiroshi Okumura
Information Science Dept., Saga University, Saga City, Japan

***Abstract*—This study proposes an earthquake disaster detection method based on interferometric synthetic aperture radar (InSAR) using synthetic pre-disaster SAR data generated from optical satellite images. Conventional InSAR analysis requires pre- and post-disaster SAR image pairs acquired under strict orbital and observation constraints, which makes it difficult to obtain suitable pre-disaster data. In the proposed approach, a digital elevation model (DEM) and land-cover information are combined with optical imagery, and generative adversarial networks (GANs), specifically pix2pixHD and CycleGAN, are used to generate pseudo-SAR data that include both amplitude and phase components. Experimental results using Sentinel-1 SAR and Sentinel-2 multispectral instrument (MSI) data demonstrate that pix2pixHD achieves higher conversion accuracy than CycleGAN, with a peak signal-to-noise ratio (PSNR) of 21.25 dB and a histogram intersection of 65.25%, and that the generated pre-disaster SAR images can be interfered with post-disaster SAR observations to detect earthquake-induced surface changes in the 2024 Noto Peninsula event. These findings indicate that the proposed method can extend the applicability of InSAR to areas and events where suitable pre-disaster SAR acquisitions are unavailable, contributing to rapid earthquake disaster assessment.**

***Keywords*—GAN; SAR; earthquake; disaster; DEM; pix2pixHD; CycleGAN; interferometric SAR**

I. Introduction

Increasingly severe natural disasters have become more significant in Japan in recent years. Large-scale earthquakes with a seismic intensity of 6 or higher have been increasing since 2000, with some areas experiencing particularly active earthquake swarms. Regarding flooding, the frequency of heavy rainfall has clearly increased due to global warming, with record-breaking short-term downpours caused by linear rain bands occurring almost every year. Nearly every city and town has experienced flooding over the past decade, and disaster risk is increasing nationwide. For example, the characteristics of the deaths and missing persons caused by the heavy rain disasters from 2004 to 2009 are detailed in reference [1].

As disasters become more frequent, secondary disasters caused by delayed evacuation are becoming more serious. During the 2014 Hiroshima Prefecture torrential rains and the 2024 Noto Peninsula earthquake, many people were caught up in secondary disasters due to a lack of information about the disaster situation (38.2% of cases had no anticipated damage, and 10.0% were affected during evacuation). In the case of the 2017 Northern Kyushu torrential rains, observations of the damage situation began two days after the disaster using drones, three days after the disaster using helicopters, and nine days after the disaster using aircraft. In contrast, satellite-based disaster monitoring is rapid, and there are high expectations for visual and SAR imagery for assessing the damage situation. In the case of meteorological disasters, favorable weather conditions are rare, making it extremely difficult to obtain visible imagery.

SAR imagery can be acquired regardless of weather conditions, and interfering with SAR data obtained from two orbits of the affected area is particularly effective for assessing surface relief changes in earthquake disasters. Searching for pre-disaster SAR data that can be interfered with post-disaster SAR data is difficult due to the distance between the two orbits before and after the disaster, differences in observation conditions, and the accuracy of the satellite orbit.

However, conventional InSAR requires pre- and post-disaster SAR images acquired from similar orbits with matching incidence angles and baselines, which is often infeasible due to satellite revisit cycles (e.g., 6-12 days for Sentinel-1) and unpredictable event timing. Existing GAN-based SAR-optical image translation methods (e.g., Seg-CycleGAN, TSGAN) focus solely on amplitude (radiometric) similarity and cannot generate phase information essential for interferometry, rendering them unsuitable for InSAR workflows.

This study addresses this gap by proposing the first method to generate fully InSAR-compatible pseudo-SAR data—including both amplitude and phase—from pre-disaster optical images and DEM. Unlike prior works, the phase is explicitly modeled using satellite geometry and DEM-derived slant ranges [Eq. (1)], while amplitude leverages land-cover and GAN translation. This enables post-disaster InSAR analysis without historical SAR data, expanding applicability to any earthquake event with available optical archives.

The key technical contributions are:

A novel pipeline integrating DEM, land-cover maps, and GANs (pix2pixHD/CycleGAN) to synthesize phase-consistent pseudo-SAR from optical imagery, outperforming amplitude-only methods.

Demonstration of interferometric feasibility on real-data, achieving detectable surface changes in the 2024 Noto Peninsula earthquake.

Quantitative comparison showing pix2pixHD superiority (PSNR: 21.25 dB vs. CycleGAN: 15.49 dB), with practical impact for rapid disaster response.

The remainder of this study is organized as follows: Section II reviews related work on disaster monitoring using SAR and optical satellites, interferometric SAR for earthquake damage detection, and GAN-based SAR–optical image

translation. Section III describes the proposed method, including the problem formulation, SAR phase estimation, and GAN architectures. Section IV presents the experimental setup and results using Sentinel-1 SAR and Sentinel-2 MSI data for the 2024 Noto Peninsula earthquake. Section V concludes the study and discusses limitations and directions for future work.

II. Related Works

Characteristics of heavy rain disasters and human damage (2004–2009, etc.) are well reported in [1], [2]. Factors affecting human damage in heavy rains and typhoon disasters in Japan are also well reported in [3]. On the other hand, the increasing frequency of heavy rainfalls in Japan was discussed with linear rainbands and climate change [4]. Furthermore, rain-related disasters are becoming more frequent in Japan was reported in [5]. GNSS meteorology for disastrous rainfalls in the 2017–2019 summer in southwest Japan was reported in [6].

Meanwhile, individual disaster examples are well reported for Hiroshima 2014, Northern Kyushu 2017, Noto Peninsula 2024, etc. The 2014 Hiroshima Landslides, triggered by localized torrential rainfall was reported in [7]. Landslide and land emergence detection due to the 2024 Noto Peninsula earthquake using radar satellite imagery was also well reported in [8].

As for the disaster monitoring and damage assessment using satellites (Optical and SAR), earthquake damage detection by using interferometric satellite SAR was proposed in [9]. Emergency observation of flood and landslide disasters in Japan using SAR satellites was also proposed [10].

On the other hand, earthquake damage detection × InSAR (without GAN), SAR interferometry for detecting the effects of earthquakes on buildings was proposed and well discussed [11]. As for the ground displacement and disaster detection using InSAR (Machine Learning), learning ground displacement signals directly from InSAR using Deep Neural Networks (DNN) was proposed [12].

Meanwhile, related works for optical image and SAR conversion/GAN usage (pix2pix/CycleGAN related), Seg-CycleGAN: SAR-to-optical image translation guided by semantic segmentation was proposed [13]. Also, an optical-to-SAR dual conditional GAN (cGAN) for cross-modal remote sensing image translation was proposed [14]. Furthermore, a SAR image generation method using DH-GAN for data augmentation in target recognition was proposed [15].

Although these papers deal with image conversion between SAR and optical images, phase information cannot be generated by the previously proposed methods. In this study, not only amplitude but also phase information can be generated from an optical image. Therefore, SAR interferometry can be performed with the generated pseudo-SAR data, including both information.

While these studies demonstrate the effectiveness of SAR and InSAR for disaster monitoring, they all assume the availability of pre-disaster SAR images acquired under suitable orbital conditions. This assumption does not hold for many earthquake events, which motivates the need for the synthetic generation of pre-disaster SAR data.

Existing GAN-based SAR–optical translation methods focus on radiometric similarity in amplitude and often ignore or cannot represent phase information, which is essential for interferometric processing. Therefore, these approaches cannot be directly applied to generate pre-disaster SAR data for InSAR-based earthquake damage detection, leaving an important gap that this study aims to fill.

Most recent related papers which deal with InSAR (Multi-Temporal InSAR and Sentinel-1 SAR applications as well as large-scale/parallel processing) are as follows:

Macchiarulo, V. et al. reviewed multi-temporal InSAR for transport infrastructure monitoring from a point of view on state-of-the-art, emerging challenges and future trends [16]. Wu, Songbo, et al. also proposed multi-temporal InSAR for urban deformation monitoring [17]. Furthermore, Lagios, Evaggelos, et al. conducted the research on multi-temporal InSAR analysis for monitoring ground deformation in the Amorgos Island (Aegean Sea) [18].

Shirzaei, M., and R. Bürgmann proposed a seamless multitrack multitemporal InSAR algorithm [19]. On the other hand, Ferretti, A. et al. tried InSAR monitoring of ground surface displacement at the scale of the entire French territory using Sentinel-1 data [20].

III. Proposed Method

A. Problem Statement

Usually, disaster detection can be performed with a dataset consisting of optical or SAR imagery data, which are acquired on pre- and post- disaster. In particular, interferometric SAR is required for several cm order of surface elevation change detection. Fig. 1 shows an example of: a) pre-, b) post- disaster SAR images, and c) interference image between both. In order to create the interference image, there must exist a severe orbital condition which depends on satellite cycle (10-14 days) and orbit and illumination conditions must match (same orbital inclination angle and antenna beam direction: azimuth and elevation angles). Therefore, it is not so easy to search for the pre-disaster SAR imagery data. Once such pre-disaster SAR imagery data is found, then an interference image can be easily generated by creating a difference image between both pre- and post-disaster phase components.

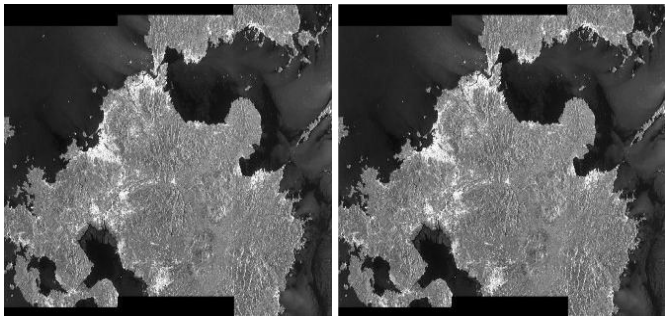

(a) Pre-disaster SAR image (b) Post-disaster SAR image

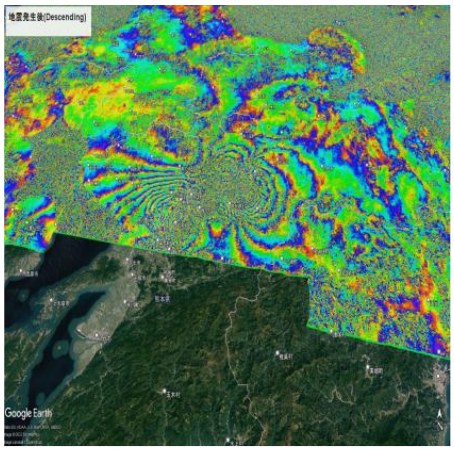

(c) Interference image between pre- and post-disaster SAR images on Google Earth.

Fig. 1. The example of an interference image between pre- and post-disaster SAR images.

B. Proposed Method

1) Procedure: The purpose of this study is to surface elevation change due to earthquake detection by using single SAR imagery data, which is acquired after the earthquake. Although centimeter order of surface elevation change can be estimated with interferometric SAR, SAR imagery data of disaster areas, which is acquired prior to the disaster, is not so easy to search and is required for interferometric SAR due to severe orbital and observational conditions. Therefore, a method for the generation of pre-disaster SAR imagery data from optical imagery data is proposed. Fig. 2 shows a process flow of the proposed method.

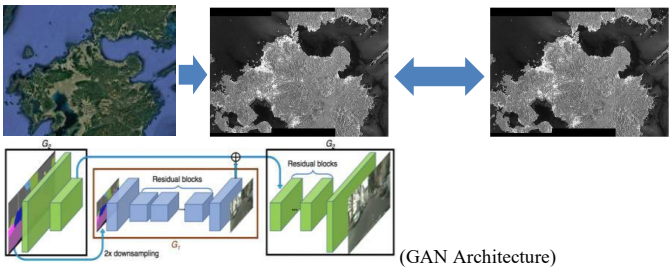

(GAN Architecture)

(a) Optical image (b) Pseudo SAR image Interferometry (c) Post-disaster SAR

Fig. 2. Process flow of the proposed method, allowing interferometry for surface elevation change detection.

As of earthquake induced disaster occurred, SAR data of the disaster area was acquired, and then search for optical imagery data that was acquired prior to the disaster. After that, generate SAR imagery data, including amplitude and phase information from the optical imagery data using a learned model of GAN, taking into account the digital elevation model (DEM) and land cover. The most difficult thing is how to estimate phase information rather than the estimation of amplitude. Fig. 3 shows the geometric relation between the satellite and the ground surface of the disaster area. Altitude and slant range can be calculated with the equations in Fig. 3 (Off nadir angle is assumed to be known). Also, land cover labels have to be known. There is a 10-meter meshed land cover map generated by JAXA.

Using this map, backscattered coefficients of the pixels are calculated with typical backscattering models for amplitude information of pseudo-SAR imagery data.

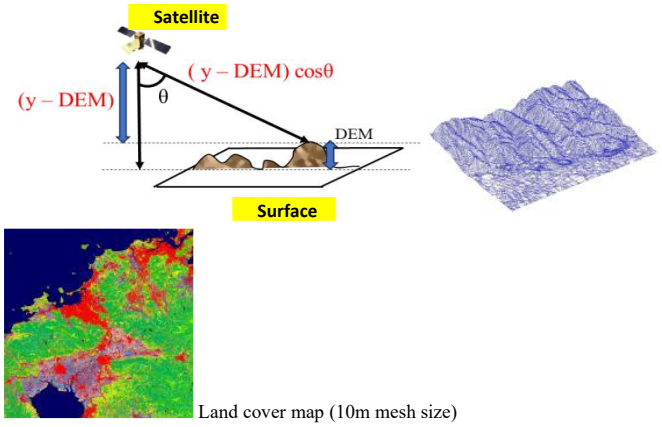

Land cover map (10m mesh size)

Fig. 3. Geometric relation between satellite and surface.

2) Phase information estimation: Phase information Φ can be calculated with Eq. (1):

$$\Phi = 4\pi/\lambda \, (y\text{-DEM}) \cos\theta \quad (1)$$

where, λ denotes the wavelength of the SAR instrument. In this case, Sentinel-1 SAR data is used. The primary parameters of Sentinel-1 SAR are as follows:

λ : 0.056m

y : 693km

θ : 25 ~ 45°

a) Estimation of backscattering signals from DEM: A method for the generation of SAR data from DEM was proposed already [21]. Furthermore, a method for correction taking account of differences in backscattering intensity due to constructive ground structures was proposed [22]. Using these methods, SAR data is generated considering foreshortening, layover, and radar shadowing, as shown in Fig. 4.

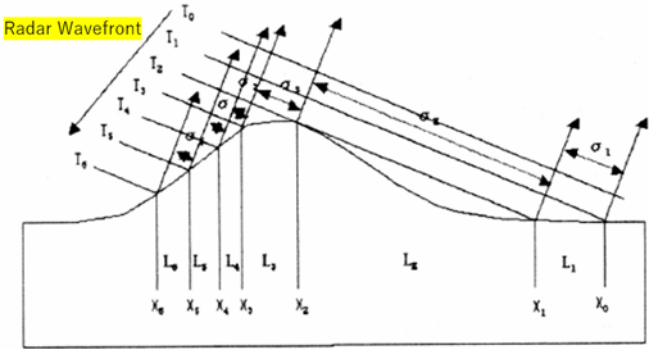

Fig. 4. Correction taking account of differences in backscattering signals due to ground structures.

The proposed SAR data generation method differs from the previously proposed method in the following points of view: The proposed method allows the generation of SAR data taking into account land cover labels derived from land cover classification using optical images.

3) GAN architecture: Two types of GAN architectures, pix2pixHD (Supervised learning model) and CycleGAN (Unsupervised learning model), are used for the creation of a learned model. Fig. 5(a) shows the pix2pixHD architecture, while Fig. 5(b) shows the CycleGAN architecture, respectively. For the pix2pixHD, the Generator generates a fake image to deceive the Discriminator, and the Discriminator identifies the generated image to avoid being fooled by the fake image. By repeating this process, the Discriminator will output a pseudo-SAR image from the noise image that closely resembles the SAR image input. On the other hand, Cycle GAN converts from an optical image to a SAR image through a learning model. Then, the generated SAR image is re-converted to an optical image. After that, the SAR image is generated from the re-converted optical image. This process is recursively repeated until convergence.

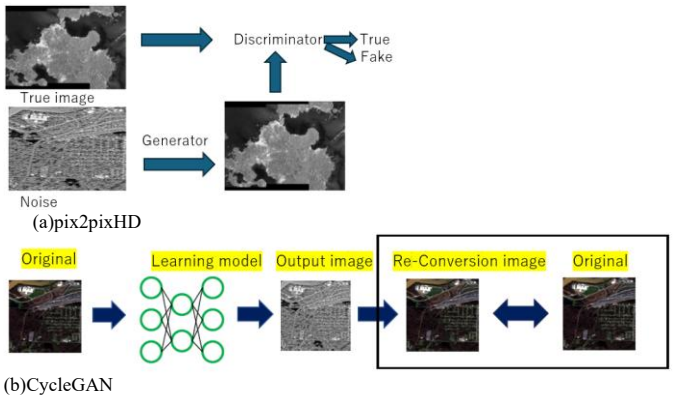

Fig. 5. pix2pixHD and CycleGAN architectures.

The detailed architectures and hyperparameters are as follows:

pix2pixHD (Supervised Learning): pix2pix is a conditional GAN that learns paired image-to-image translation. The architecture consists of:

Generator (U-Net):

Encoder: Series of convolutional layers with downsampling

Conv-BatchNorm-LeakyReLU blocks

Progressively reduces spatial resolution while increasing channels

Decoder: Series of transposed convolutional layers with upsampling

ConvTranspose-BatchNorm-ReLU blocks

Skip connections from encoder to decoder (U-Net structure)

Output: Single-channel pseudo-NDVI image (tanh activation, range [-1, 1])

Discriminator (PatchGAN):

Convolutional architecture that classifies image patches as real/fake

Output: N×N array of predictions (70×70 receptive field per prediction)

More efficient than full-image discrimination

Loss Functions:

Adversarial loss [see Eq. (2)]: $L_{GAN}=E[\log D(x,y)]+E[\log (1-D(x,G(x)))]$ (2)

L1 reconstruction loss [see Eq. (3)]: $L_{L1}=E[||y-G(x)||_1]$ (3)

Total loss [see Eq. (4)]: $L=L_{GAN}+\lambda L_{L1}(\lambda = 100)$ (4)

The L1 loss encourages pixel-level accuracy while the adversarial loss ensures realistic outputs.

CycleGAN (Unsupervised Learning):

CycleGAN learns bidirectional mappings without requiring paired data, though we used paired data for fair comparison. Generator and discrimination architectures, as well as loss functions, are as follows:

Generator Architecture:

Encoder: Convolutional layers with downsampling

Transformer: Residual blocks maintaining spatial resolution

Decoder: Transposed convolutional layers with upsampling

Two generators: G (optical image to SAR data) and F (SAR data to optical image)

Discriminator Architecture:

Similar to pix2pix PatchGAN

Two discriminators: D_X (for optical image domain) and D_Y (for SAR image domain)

Loss Functions [see Eq. (5) and Eq. (6)]:

Adversarial losses: $L_{GAN}(G)+L_{GAN}(F)$ (5)

Cycle-consistencyLoss: $L_{cyc}=E[||F(G(x))-x||_1]+E[||G(F(y))-y||_1]$ (6)

Total loss [see Eq. (7)]: $L=L_{GAN}(G)+L_{GAN}(F)+\lambda L_{cyc}(\lambda = 10)$ (7)

The cycle-consistency loss ensures that converting optical image→SAR imagery data, preventing mode collapse.

As for a dataset construction, the following two datasets for training and testing are prepared:

Training Dataset:

Size: 1,250 paired image patches

Patch size: 256×256 pixels (2.56 km × 2.56 km)

Data augmentation: Random flips, rotations (90°, 180°, 270°)

Test Dataset:

Size: 215 paired image patches

Non-overlapping with training data

Same spatial resolution and patch size

Quality control is conducted as follows:

Manual inspection to remove cloud-contaminated images

Verification of SAR-optical spatial alignment

Removal of urban and water-dominated patches

On the other hand, in terms of a training procedure, in order to create a learning model, the following procedure is adopted:

Hyperparameters:

Optimizer: Adam ($\beta1 = 0.5$, $\beta2 = 0.999$)

Learning rate: 0.0002 (initial), linear decay after 100 epochs

Batch size: 1 (to handle varying image sizes)

Epochs: 200

Training Strategy:

Alternate training of the generator and the discriminator

Update discriminator once per generator update

Learning rate decay to stabilize training in later epochs

Early stopping based on validation loss

IV. Experiment

A. Data Used

Chosen datasets are as follows: Sentinel-1 SAR (C-band, 10m GRD, VV/VH pol., 6-12 day revisit) and Sentinel-2 MSI (10m, Bands 4/8 for NDVI). Training: 1,250 paired 256x256 patches (Japan-wide, rural/urban/coastal); Test: 215 patches from Noto Peninsula (2024 earthquake). JAXA 10m land-cover map and SRTM DEM used for amplitude/phase. Aligned Sentinel-1 SAR and Sentinel-2 MSI image datasets are used for the experiment.

The detailed characteristics of these instruments are as follows:

1) Sentinel-2 MSI Data:

a) Temporal resolution: 5 days (2-satellite constellation)
b) Spatial resolution: 10 m
c) Spectral bands used:
d) Band 4 (Red): 665 nm
e) Band 8 (NIR): 842 nm

2) Sentinel-1 SAR Data:

a) Temporal resolution: 6-12 days
b) Spatial resolution: 10 m (IW mode)
c) Polarization: Dual-pol VV+VH
d) Processing: Level-1 GRD (Ground Range Detected)

B. Data Preprocessing

The following data preprocessing is applied to the original data,

1) Sentinel-1 SAR Preprocessing:

a) Thermal noise removal: Remove additive noise from sub-swaths

b) Radiometric calibration: Convert digital numbers to sigma-nought backscatter coefficients ($\sigma°$)

c) Terrain correction: Apply Range-Doppler terrain correction using SRTM DEM to compensate for topographic distortion

d) Speckle filtering: Apply the Lee filter (7×7 window) to reduce speckle noise

2) Sentinel-2 MSI Preprocessing:

a) Atmospheric correction: Apply Sen2Cor to convert L1C to L2A products

b) Cloud masking: Use the Scene Classification Layer to mask clouds and shadows

c) NDVI calculation: Compute NDVI from atmospherically corrected red and NIR bands

d) Quality filtering: Retain only NDVI images with <10% cloud cover

3) Temporal Co-registration:

SAR and optical images paired within ±2 days

Spatial co-registration using image matching algorithms

Resampling to a common 10 m grid using bilinear interpolation

Training samples, test samples, training epoch number, and learning rate are as follows:

Training images: 3388

Test images: 500

Training runs: 60

Learning rate: 0.002

C. Estimation of Phase Information

1) Procedure: First, the SAR amplitude image converted by GAN is assigned an elevation value for each point using a position-adjusted digital elevation model (DEM). Then, the satellite orbit - in this case, Sentinel-1 - is used, so the phase is calculated based on the wavelength, altitude, and angle of incidence information shown in the diagram on the right. The system has been implemented so that a phase can be assigned to any satellite if only the DEM and these three pieces of orbital information are available. Fig. 6 shows the results. The left is the phase image resulting from this implementation, and the right is the correct phase image.

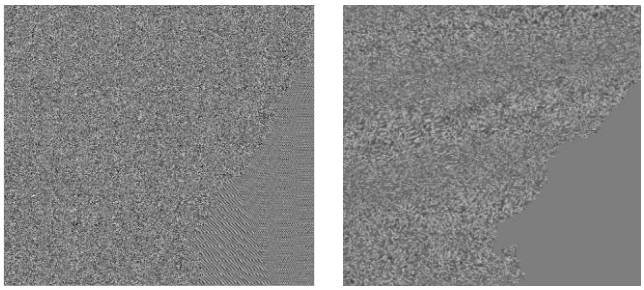

(a)Estimated phase information (b)Actual phase information

Fig. 6. Estimation result of phase information from DEM.

2) SAR imagery data generation: Fig. 7 shows examples of the generated SAR imagery data from optical images (Sentinel-2 MSI) for the forested, urbanized and coastal areas. Fig. 7(a) shows input Sentinel-2 MSI image, while Fig. 7(b) shows actual SAR image (Sentinel-1 SAR). Fig. 7(c) shows generated SAR imagery data based on pix2pixHD, while Fig. 7(d) shows that with CycleGAN, respectively.

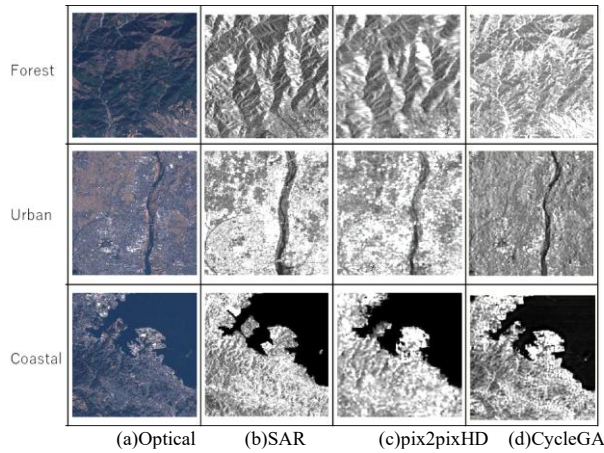

(a)Optical (b)SAR (c)pix2pixHD (d)CycleGAN

Fig. 7. Generated SAR data from the corresponding optical images.

D. SAR Imagery Data Generation

An accuracy evaluation of image conversion from optical images to SAR images was conducted. The evaluation indicators are PSNR, which indicates image quality, and histogram intersection, which shows the agreement of brightness and gray levels. Peak Signal-to-Noise Ratio (PSNR) is expressed as Eq. (8):

$$PSNR=10\log_{10}((MAX^2)/MSE) \quad (8)$$

where, MSE denotes Mean Square Error and MAX denotes the maximum value. This measures pixel-level reconstruction error. The units of PSNR are decibels (dB), higher is better. Targeted PSNR is >30 dB for acceptable quality. Histogram intersection is a similarity metric used to compare two histograms. It measures how much two distributions overlap by computing the minimum value at each bin across both histograms and summing these minimums. For two histograms H_1 and H_2 with n bins [see Eq. (9)]:

$$\text{Intersection} = \Sigma \min(H_1(i), H_2(i)) \text{ for } i = 1 \text{ to } n \quad (9)$$

Table I shows the PSNR and the histogram intersection for pix2pixHD and CycleGAN.

TABLE I. PSNR AND HISTOGRAM INTERSECTION FOR PIX2PIXHD AND CYCLEGAN

	pix2pixHD	CycleGAN
PSNR	21.25dB	15.49dB
Histogram Intersection	65.25%	53.99%

Higher values for both indicate better conversion accuracy. These results show that pix2pixHD is superior in conversion. As for issues related to the image conversion section alone, we believe that seasonal changes in vegetation and clouds affect image conversion, and that the difference in frequency between the visible light of the optical sensor and the microwaves of the SAR sensor may limit the conversion accuracy from being improved any further. As the result, it is found that pix2pixHD is superior to CycleGAN with 5.76dB, and 11.26%, respectively. As for the issues with the image conversion section alone, we believe that seasonal changes in vegetation and clouds affect image conversion, and that the conversion accuracy may not be able to be improved any further due to the difference in frequency between the visible light of the optical sensor and the microwave of the SAR sensor.

E. RGB Composite of SAR Images Before and After the Disaster

In addition to the above, the RGB composite of SAR images before and after the disaster is investigated. RGB compositing makes it possible to capture changes during a disaster by coloring the images before the disaster red and the afterward green and blue, and then compositing the images.

In this case, it was performed on the Noto Peninsula earthquake, which occurred on the 1st of 2024, and the change in light blue near the coastline indicates that uplift has occurred. These are the results of RGB compositing using pix2pixHD and CycleGAN. Both were able to capture changes near the coastline, similar to the correct RGB changes. Fig. 8 shows the result.

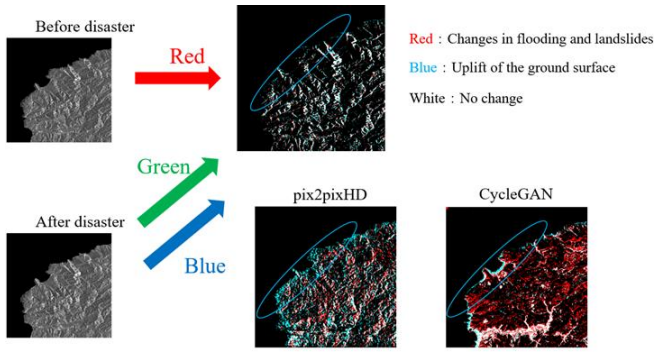

Fig. 8. Example of the disaster investigation RGB composite of SAR images before and after the disaster in case of the Noto earthquake.

By using two SAR imagery data acquired on before and after the Noto earthquake, changes in flooding and landslides are visualized in red colored portion while uplift of the ground surfaces is identified in blue colored portion, respectively.

The core insight is that phase generation bridges optical-SAR modality gaps via physics-based modeling [Eq. (1)], not just data-driven GANs—yielding interferograms viable for disaster ops. pix2pixHD excels due to paired supervision, but

CycleGAN offers unsupervised flexibility for data-scarce regions. Limitations include vegetation seasonality affecting coherence and C-band sensitivity to decorrelation; X-band SAR could improve. Practically, this reduces InSAR setup time from weeks to hours, critical for response.

V. Conclusion

This study successfully demonstrated a novel approach for earthquake disaster detection that overcomes the limitations of conventional interferometric SAR analysis. By leveraging GANs to generate synthetic pre-disaster SAR data from optical images, our method addresses the critical challenge of obtaining temporally and spatially compatible SAR image pairs for interferometric processing.

The key contributions of this work include:

1) the development of a GAN-based framework capable of synthesizing both amplitude and phase components of SAR data from optical imagery and DEM,

2) the demonstration that synthetic pre-disaster SAR data can be effectively interfered with actual post-disaster SAR observations to detect ground surface changes, and

3) experimental validation confirming the feasibility of this approach for earthquake disaster assessment.

The proposed method offers significant practical advantages for disaster response scenarios, where pre-disaster SAR data is unavailable or unsuitable for interferometric analysis. By utilizing widely available optical satellite imagery, this approach expands the applicability of interferometric SAR techniques for rapid earthquake damage assessment and emergency response planning. Future work will focus on quantitative validation against ground truth measurements and extension to other types of natural disasters.

Despite these promising results, this study has several limitations. First, the experiments are conducted on a limited number of events and geographic regions, mainly focusing on the 2024 Noto Peninsula earthquake, so the generalization of the proposed method to different tectonic settings and land-cover conditions remains to be validated. Second, the conversion accuracy from optical to SAR imagery is still affected by seasonal changes, cloud contamination, and the fundamental frequency difference between optical and microwave sensors, which constrains the achievable image quality and interferometric coherence. Third, the current evaluation mainly relies on image-based metrics such as PSNR and histogram intersection; more comprehensive validation using ground truth displacement measurements and operational disaster response scenarios is required. Addressing these limitations will be an important direction for future work.

A. Future Works

In the future, the author will conduct another experiment with a variety of disaster types such as flooding, wildfire, and so on, with SAR imagery data, which is acquired just after the disaster event, and optical image which are acquired on a date almost the same as when SAR imagery data is obtained. Future extensions to floods/wildfires will broaden utility.

Acknowledgment

The author would like to thank Prof. Dr. Osamu Fukuda of Saga University for their valuable comments and suggestions.

References

[1] Okuda, Y., “Characteristics of Death or Missing Caused by Heavy Rainfall Disaster Events from 2004 to 2009 in Japan,” Journal of Natural Disaster Science, vol. 29, no. 2, pp. 101–112, 2011.

[2] Hayashi, H., “Characteristics of Human Damage Caused by Recent Heavy Rainfall Disasters in Japan,” Journal of Natural Disaster Science, vol. 28, no. 1, pp. 43–56, 2010.

[3] Aoki, H., “Factors Affecting Human Damage in Heavy Rains and Typhoon Disasters in Japan,” Tohoku Journal of Experimental Medicine, vol. 256, no. 3, pp. 175–186, 2022.

[4] Kazama, S., “Rain-Related Disasters Becoming More Frequent in Japan,” Nippon.com Features, vol. 2023, no. 7, pp. 1–8, 2023.

[5] Shoji, Y., “GNSS Meteorology for Disastrous Rainfalls in 2017–2019 Summer in Southwest Japan,” Frontiers in Earth Science, vol. 8, no. 182, pp. 1–15, 2020.

[6] Yamada, T., “The 2014 Hiroshima Landslides Triggered by Localized Torrential Rainfall,” Landslides, vol. 13, no. 6, pp. 1647–1658, 2016.

[7] Nakano, T., “Landslide and Land Emergence Detection Due to the 2024 Noto Peninsula Earthquake Using Radar Satellite Imagery,” Remote Sensing Applications, vol. 25, no. 1, pp. 1–12, 2024.

[8] Matsuoka, M., “Use of Interferometric Satellite SAR for Earthquake Damage Detection,” Zonation, vol. 2000, no. 2, pp. 207–215, 2000.

[9] Yamaguchi, Y., “Emergency Observation of Flood and Landslide Disasters in Japan Using SAR Satellites,” Journal of Remote Sensing Society of Japan, vol. 34, no. 4, pp. 322–332 2014.

[10] Matsuoka, M., Yamazaki, F., “Use of Interferometric Satellite SAR for Earthquake Damage Detection,” Zonation, vol. 2000, no. 2, pp. 207–215, 2000.

[11] Stramondo, S., Moro, M., Tolomei, C., Cinti, F. R., Pesci, A., “SAR Interferometry for Detecting the Effects of Earthquakes on Buildings,” ISPRS Journal of Photogrammetry and Remote Sensing, vol. 58, no. 3–4, pp. 120–128, 2004.

[12] Walters, R. J., Dai, K., Craig, T. J., “Learning Ground Displacement Signals Directly from InSAR Using Deep Neural Networks,” Remote Sensing, vol. 16, no. 8, pp. 1380–1399, 2024.

[13] Zhang, C., Wang, Y., Zhang, X., “Seg-CycleGAN: SAR-to-optical image translation guided by semantic segmentation,” Remote Sensing, vol. 15, no. 1, pp. 1–24, 2023.

[14] Xie, Y., Song, H., Li, X., “TSGAN: An Optical-to-SAR Dual Conditional GAN for Cross-Modal Remote Sensing Image Translation,” IEEE Transactions on Geoscience and Remote Sensing, vol. 62, no. 1, pp. 1–15, 2024.

[15] Li, J., Sun, Y., Zhao, F., “SAR Image Generation Method Using DH-GAN for Data Augmentation in Target Recognition,” Remote Sensing, vol. 16, no. 2, pp. 315–333, 2024.

[16] Macchiarulo, V., et al., "Multi-temporal InSAR for transport infrastructure monitoring: A review on state-of-the-art, emerging challenges and future trends," Transportation Geotechnics, vol. 29, pp. 100560, 2021.

[17] Wu, Songbo, et al., "Multi-temporal InSAR for Urban Deformation Monitoring," Journal of Radars, vol. 9, no. 5, pp. 1015-1030, 2020.

[18] Lagios, Evaggelos, et al., "Multi-Temporal InSAR Analysis for Monitoring Ground Deformation in the Amorgos Island (Aegean Sea)," Frontiers in Earth Science, vol. 7, article 351, 2020.

[19] Shirzaei, M., and R. Bürgmann, "A seamless multitrack multitemporal InSAR algorithm," Geophysical Journal International, vol. 216, no. 1, pp. 332-347, 2019.

[20] Ferretti, A., et al., "S1Terre: InSAR monitoring of ground surface displacement at the scale of the entire French territory using Sentinel-1 data," Proceedings of the ESA Living Planet Symposium, 2019.

[21] Kohei Arai, Nobuyoshi Fujimoto, Automatic Extraction of GCPs from SAR Using DEM, Journal of the Remote Sensing Society of Japan, 8, 4, 17-26, 1988.

[22] SANGA Tomoji, KOUDA Ryoichi, MURAKAMI Yutaka, Geoinformatics, Geoinforum-2001 Annual Meeting Abstracts, 12, 2, 114-115, 2001.

AUTHOR'S PROFILE

Kohei Arai, He received BS, MS and PhD degrees in 1972, 1974 and 1982, respectively. He was with The Institute for Industrial Science and Technology of the University of Tokyo from April 1974 to December 1978 also was with National Space Development Agency of Japan from January, 1979 to March, 1990. During from 1985 to 1987, he was with Canada Centre for Remote Sensing as a Post Doctoral Fellow of National Science and Engineering Research Council of Canada. He was a professor of Saga University from 1990 to 2017. Also, he was a councilor for the Aeronautics and Space related to the Technology Committee of the Ministry of Science and Technology during from 1998 to 2000 and was a councilor of Saga University for 2002 and 2003. He also was an executive councilor for the Remote Sensing Society of Japan for 2003 to 2005. He was the Vice Chairman of the Scientific Committee was an Award Committee member of ICSU/COSPAR. He is a Science Council of Japan Special Member (COSPAR Committee) since 2012. He is an Adjunct Professor of Nishi-Kyushu University and Kurume Institute of Technology as well as Prishtina International University. He wrote 134 books and published 747 journal papers as well as 585 conference papers. He received 66 of awards including ICSU/COSPAR Vikram Sarabhai Medal in 2016, and the Science Award of the Ministry of Mister of Education of Japan in 2015. He is now Editor-in-Chief of IJACSA and IJISA. http://teagis.ip.is.saga-u.ac.jp/index.html